

# Analysis of spatial light modulator contrast ratios and optical correlation

Peter D. Gianino, Charles L. Woods, and Joseph L. Horner

We have performed a general analysis of optical correlators with spatial light modulators (SLM's) whose primary defect is a finite contrast ratio (CR). Our mathematical analysis identifies three noise terms that appear in addition to the correlation term. The filter SLM contains either a phase-only filter (POF) or a binary-phase-only filter (BPOF). Insertion of a dc block at the center of the filter SLM decreases the noise background in the correlator plane; this dc block is larger than that required for the same level of performance in a correlator whose SLM's have transmissive (or reflective) dead zones. With a noise-free input and the dc block, our computer simulations that show the peak intensity falling off as the CR decreases are in quantitative agreement with the correlation term of the mathematical model. For a cluttered, disjoint noise input this agreement is only qualitative, and at low CR's the dc block is definitely required for the BPOF correlator if the secondary peaks in the output are to be brought below the correlation peak.

## 1. Introduction

In most of the analyses performed on optical correlators two assumptions are usually made about the spatial light modulators (SLM's) used in the system: (1) that the modulator's pixels have no dead zones that could impair the transmission of signals, and (2) that these pixels perfectly modulate the readout light through their active zones, that is, they have an infinite contrast ratio (CR). In previous publications<sup>1-3</sup> we examined the effects that the different types of dead zones have on optical-correlator performance. In this paper we study the effects of an SLM's finite CR on optical correlation.

The CR for an amplitude-modulated SLM is defined as the ratio of the maximum intensity transmitted through (or reflected off) the SLM when turned on ( $I_{ON}$ ) to the maximum intensity transmitted through (or reflected off) the SLM when turned off ( $I_{OFF}$ ).<sup>4</sup> Mathematically, this contrast ratio  $R$  can be written as

$$R = I_{ON}/I_{OFF}. \quad (1)$$

For a SLM that perfectly controls the light,  $I_{OFF}$

vanishes, so  $R$  is infinite. For a real SLM with less-than-perfect control over the light,  $I_{OFF}$  is non-zero, so  $R$  becomes finite.

Typical values of CR's for current SLM's are in the range of 10 to 50.<sup>5,6</sup> Reference 6 lists CR values from  $10^4$  down to 2 that are associated with different SLM's. Davis *et al.*<sup>7</sup> reported CR values for Semetex magneto-optic spatial light modulators that were between 2300 and 45,000. They found a surprising variation in the CR when tilt in the magneto-optic layer and rotation of the sample were present. Other workers have reported various values of CR's for different types of SLM's under a variety of conditions.<sup>7-10</sup> A high CR is obviously desired for display purposes. But up to now, it has not been clear whether a high CR, with its attendant high cost, was necessary for optical processing.

In this study we confined our investigations only to the standard 4- $f$  correlators with either a phase-only or a binary-phase-only filter on the transform plane SLM. In the mathematical model of these SLM's we show that three noise terms appear; they represent noise contributions that interfere with the principal correlation pattern in a manner similar to that reported in our previous analysis of dead zones.<sup>2,3</sup> Correlators having finite-CR SLM's experience smaller losses to the off-axis (that is, higher-order) patterns relative to those correlators with finite dead-zone SLM's.

The authors are with Rome Laboratory, U.S. Air Force, Hanscom Air Force Base, Massachusetts 01731-6346.

Received 11 March 1994; revised manuscript received 5 May 1995.

0003-6935/95/296682-13\$06.00/0.

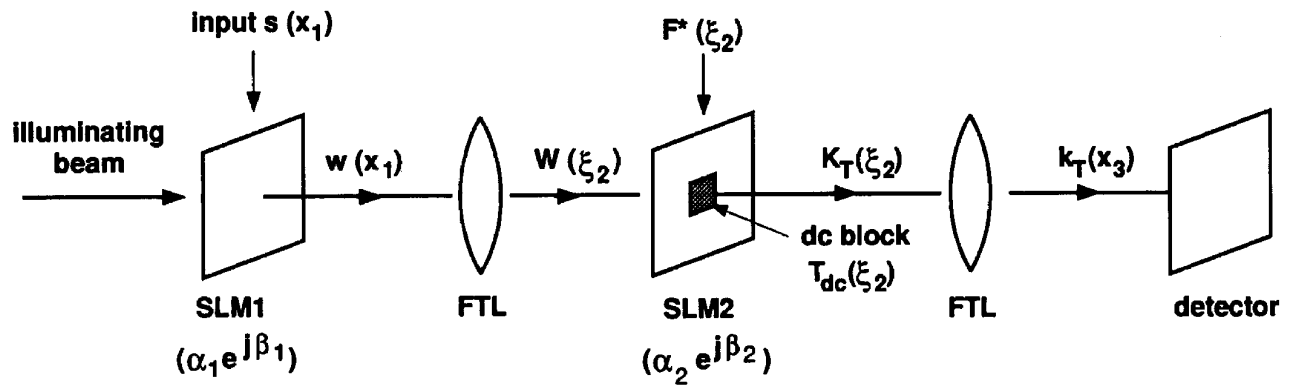


Fig. 1. Standard 4- $f$  correlator with SLM's in both the input and filter planes and a dc block in the filter SLM. All other expressions are explained in the text.

## 2. CR Models for SLM's

In this section we quantitatively determine the operation of correlators with finite CR's. We assume that all of the pixels of a given SLM are uniform (see Section 3). This enables one to calculate the potential improvement in performance that is provided solely by an improvement in the CR.

Figure 1 shows a standard 4- $f$  correlator. SLM1 and SLM2 represent spatial light modulators comprising the input and filter planes, respectively, and the FTL's represent Fourier-transforming lenses. A unit-amplitude readout plane wave illuminates SLM1. The normalized input signal (derived from the input scene) addressing SLM1 is given by  $s(x_1)$ , where  $x_1$  is the spatial coordinate in the input plane. (For purposes of simplicity, the functions shown in Fig. 1, as well as in the following analysis, are expressed in one dimension, although they can easily be extended to two dimensions.) The filter function addressing SLM2 is given by the conjugated reference function  $F^*(\xi_2)$ , where  $\xi_2$  is the spatial-frequency coordinate in the filter plane and the asterisk denotes complex conjugation. The complex transfer-characteristic function for the pixels in the  $i$ th SLM is given by  $\alpha_i \exp(j\beta_i)$ , where  $\alpha_i$  and  $\beta_i$  are real numbers.

For plane-wave illumination the approximate expression for the discrete output  $w(x_1)$  of SLM1 can be given as

$$w(x_1) \cong \alpha_1(x_1) \exp[j\beta_1(x_1)] \text{rect}\left(\frac{x_1}{L_1}\right), \quad (2)$$

where the function  $\text{rect}(x_1/L_1)$  accounts for the spatial extent  $L_1$  of SLM1. (The exact expressions for all the discrete signals dealt with in this paper are given in Appendix A). Because SLM1 is an amplitude modulator, not a phase modulator, we take  $\beta_1 = 0$ . (For SLM2,  $\beta \equiv \beta_2$  will not be zero. Also, the case when  $\beta_1 \neq 0$  has been treated in Ref. 11.) When  $s$  is unity, that is, when the pixel is turned fully on, the amplitude of the characteristic function  $\alpha_1$  is unity. When  $s$  is zero, that is, when the pixel is supposed to be turned fully off,  $\alpha_1$  does not vanish. We designate this minimum-amplitude value as  $(\alpha_1)_{\min}$ .

If we assume that  $\alpha_1$  varies linearly with  $s$ , as shown in Fig. 2(a), then

$$\alpha_1 = [1 - (\alpha_1)_{\min}]s + (\alpha_1)_{\min}. \quad (3)$$

If the constant  $1 - (\alpha_1)_{\min}$  is defined as  $c_1$ , then the

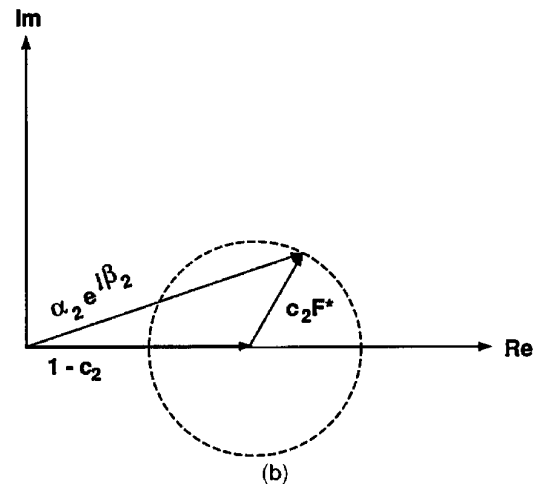
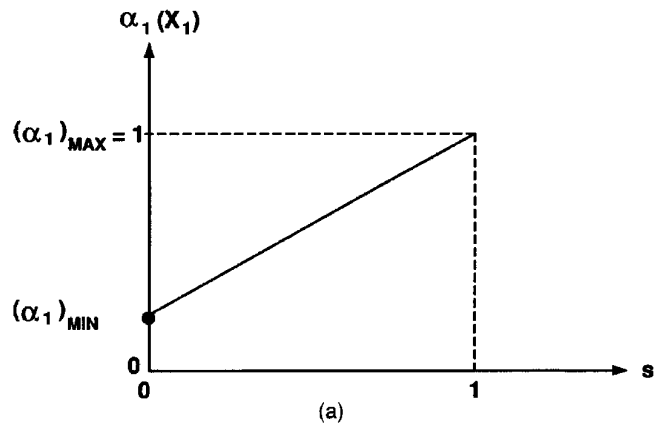


Fig. 2. Transfer characteristics for (a) the input SLM and (b) the filter SLM obtained through the use of the linearized identical-pixel model. In (a)  $\alpha_1$  is plotted against the input signal  $s$  with  $\beta_1 = 0$ . In (b) the transfer characteristics is plotted in the complex plane as a function of the filter input signal  $F^*$ .

output signal of SLM1 can be written as

$$w(x_1) = [c_1 s(x_1) + (1 - c_1)] \text{rect}\left(\frac{x_1}{L_1}\right), \quad (4)$$

where  $c_1$  is the input-signal amplitude transmittance and  $(1 - c_1)$  is the background amplitude transmittance. The range of  $c_1$  is from 0 to 1. Consequently, the CR of SLM1 becomes

$$R_1 = \frac{|w_{\text{ON}}|^2}{|w_{\text{OFF}}|^2} = \frac{1}{(\alpha_1)_{\text{min}}^2} = \frac{1}{(1 - c_1)^2}, \quad (5)$$

or,  $(\alpha_1)_{\text{min}} = 1/\sqrt{R_1}$ . After Fourier transformation,  $w(x_1)$  becomes  $W(\xi_2)$ , which is the function illuminating the input side of SLM2

SLM2 has a spatial extent represented by  $\text{rect}(x_2/L_2)$ , with  $x_2$  as the spatial coordinate in the filter plane. But, if this plane also contains a dc block at its center that consists of  $p_2$  pixels of width  $h_2$ , then its transmission function is modified to

$$T_{\text{dc}}(x_2) = \text{rect}\left(\frac{x_2}{L_2}\right) - \text{rect}\left(\frac{x_2}{p_2 h_2}\right). \quad (6)$$

The relation between  $x_2$  and the spatial-frequency coordinate  $\xi_2$ , which is given by  $x_2 = L_1 h_2 \xi_2$ , may be used to express Eq. (6) as

$$T_{\text{dc}}(\xi_2) = \text{rect}\left(\frac{L_1 h_2 \xi_2}{L_2}\right) - \text{rect}\left(\frac{L_1 \xi_2}{p_2}\right). \quad (7)$$

For a phase-only filter (POF)  $F_{\text{POF}^*}(\xi_2) = \exp[-j\Psi(\xi_2)]$ , where  $\Psi$  is the phase of  $F^*$ . Again if one assumes an identical-pixel model for SLM2, the complex transfer characteristic  $G^*(\Psi_2)$  may also be written as

$$G(\xi_2) = [\alpha_2(\xi_2)] \exp[j\beta_2(\xi_2)] T_{\text{dc}}(\xi_2). \quad (8)$$

We analyze the following model for the CR in SLM2, which is appropriate for some SLM's. For example, for certain liquid-crystal modulators the locus of all  $G^*$  values in the complex plane has been measured to be almost a closed circle whose center has been displaced from the original along the real axis.<sup>12,13</sup> We have approximated this operating curve by the circle that is shown in Fig. 2(b) and that is represented for the POF by the model

$$G^*(\xi_2) \approx [c_2 F^*(\xi_2) + (1 - c_2)] T_{\text{dc}}(\xi_2). \quad (9)$$

The complex filter function  $F_{\text{POF}^*}$  has been compressed by a factor of  $c_2$  and has been translated from the original by an amount  $(1 - c_2)$ . Thus,  $c_2$  is the reference-signal amplitude transmittance of SLM2 and  $(1 - c_2)$  is its background amplitude transmittance. The range of  $c_2$  is also from 0 to 1. For convenience, we chose the filter contrast ratio  $R_2$  to have the same algebraic form as  $R_1$  in Eq. (5) on the

basis of the POF model of approximation (9), namely,

$$R_2 = \frac{1}{(1 - c_2)^2}, \quad (10)$$

where  $R_2$  ranges from  $\infty$  to 1.

Our ad hoc filter model is in good agreement with one of the optimum-filter models in the literature. Our POF model [approximation (9)] for the SLM transfer function is in close agreement with the transfer function determined by Juday<sup>12</sup> for an optimal-filter model. In the limit of large  $R$  or for phases near 0 or  $\pi$ , the agreement is exact. However, for  $R = 5$  an addressed phase of  $\Psi = \pi/2$  is too small by an amount of  $\pi/6.2$  relative to that calculated from the Juday<sup>12</sup> model. Studies of systematic phase errors in POF correlators indicate negligible effects for maximum phase errors of less than  $\pi/5$ .<sup>14</sup> For CR's less than 5, such corrections would be increasingly significant.

As for the binary-phase-only filter (BPOF), for which the phase angle of  $F^*$  [ $\Psi(\xi_2)$  in Fig. 2(b)] takes on values of  $\Psi_0$  or  $\Psi_0 + \pi$  only, the CR has the same qualitative meaning as for the POF and still has the physical significance of the inverse of the background intensity transmittance in Eq. (10). In addition, any two-state device with any phase difference or magnitude change may use this BPOF model.

We choose  $\Psi_0 = \pi/2$  for the BPOF that we simulate, and this binarization axis produces an exact agreement with the optimal-filter model developed by Juday.<sup>12</sup> As an example of this definition of the CR for a BPOF, choosing  $c_2 = 1/2$  and  $\Psi_0 = 0$  results in an amplitude-encoded POF<sup>15</sup> with  $G^* = 1$  or  $G^* = 0$ . Here, the minimum transmittance of zero results from the destructive interference between the signal ( $c_2 F^*$ ) and the background  $(1 - c_2)$ .

### 3. SLM Uniformity and Filter Optimization

A pixel's transmission in the OFF state is determined by various factors, such as defects, thickness variations, scattered light, imperfect polarizers, and stray reflections.<sup>5,6</sup> Certainly these flaws will vary from pixel to pixel. However, such pixel nonuniformity in a SLM may be minimized through the compensation of the signal that is addressed to each pixel. If the modulation response of each pixel has been measured experimentally, appropriate corrections may be determined for each pixel. Such compensation, for example, is used in the Rome Laboratory's staring infrared camera.<sup>16-18</sup> Here, we assume that such a compensating function has been chosen to produce the best uniformity in accordance with our modeling equations for the SLM's. For the filter SLM, these corrections would be applied to the stored data in the filter bank, and it is possible to use iterative experimental techniques to optimize filters for a particular optical-correlator device.<sup>19</sup>

The compensating function for SLM2 may also include the corrections to produce an optimal filter (such as those corrections proposed by Juday<sup>12</sup> for the

POF, BPOF, and other filters) and to reduce additive noise (such as those corrections proposed by researchers working at Rome Laboratory<sup>20</sup>). Binary and ternary SLM's are clearly more limited in their abilities in these pixel-compensation techniques. The effects of complex noise in SLM's in optical correlators have also been studied.<sup>21</sup>

#### 4. Total Correlation

When illuminated by  $W(\xi_2)$ , the output  $K_T$  of SLM2 is given by the product function

$$K_T(\xi_2) \equiv W(\xi_2) \cdot G^*(\xi_2). \quad (11)$$

The inverse Fourier transform of  $K_T$  results in the total output function  $k_T(x_3)$  at the detector, where  $x_3$  is the spatial coordinate in the output plane. By means of Eq. (4) and  $g(x_3)$ , the inverse Fourier transform of Eq. (11),  $k_T$ , becomes

$$k_T(x_3) = w(x_3) \star g^*(x_3) \equiv [c_1 s(x_3) + (1 - c_1)] \text{rect}\left(\frac{x_3}{L_1}\right) \star [c_2 f^*(x_3) + (1 - c_2) \delta(x_3)] \circ t_{dc}(x_3), \quad (12)$$

where  $f^*$  is the filter impulse-response function,  $\delta$  is the delta function, the star and the centered degree sign ( $\circ$ ) represent the correlation and convolution operations, respectively, and  $t_{dc}(x_3)$ , the inverse Fourier transform of  $T_{dc}(\xi_2)$ , is given by

$$t_{dc}(x_3) = \frac{L_2}{L_1 h_2} \text{sinc}\left(\frac{L_2 x_3}{L_1 h_2}\right) - \frac{p_2}{L_1} \text{sinc}\left(\frac{p_2 x_3}{L_1}\right). \quad (13)$$

After expanding the right side of approximation (12), we can group terms and express them as follows:

$$k_T(x_3) = k_C(x_3) + k_S(x_3) + k_R(x_3) + k_{FR}(x_3), \quad (14)$$

where

$$k_C(x_3) \equiv c_1 c_2 \left[ s(x_3) \text{rect}\left(\frac{x_3}{L_1}\right) \star f^*(x_3) \right] \circ t_{dc}(x_3) \equiv c_1 c_2 A_C(x_3), \quad (15)$$

$$k_S(x_3) \equiv c_1 (1 - c_2) \left[ s(x_3) \text{rect}\left(\frac{x_3}{L_1}\right) \right] \circ t_{dc}(x_3) \equiv c_1 (1 - c_2) A_S(x_3), \quad (16)$$

$$k_R(x_3) \equiv (1 - c_1) (1 - c_2) \text{rect}\left(\frac{x_3}{L_1}\right) \circ t_{dc}(x_3) \equiv (1 - c_1) (1 - c_2) A_R(x_3), \quad (17)$$

$$k_{FR}(x_3) \equiv (1 - c_1) c_2 \left[ \text{rect}\left(\frac{x_3}{L_1}\right) \star f^*(x_3) \right] \circ t_{dc}(x_3) \equiv (1 - c_1) c_2 A_{FR}(x_3), \quad (18)$$

The  $A_i(x_3)$  represent the  $x_3$ -dependent terms. They can refer to either the approximate expressions shown in relations (15)–(18) or the exact expressions given in

Appendix A. Equation (14) can now be written out as

$$k_T(x_3) = c_1(A_S - A_R) + c_2(A_{FR} - A_R) + c_1 c_2(A_C - A_S + A_R - A_{FR}) + A_R. \quad (19)$$

#### 5. Correlation and Noise Terms

Relations (14)–(18) show that the final output consists of a correlation term  $k_C$  and three background terms. These terms are similar to those in the analysis of correlators in which the one or both SLM's contain transmissive dead zones.<sup>2,3</sup> The primary difference for finite-CR SLM's is that a single-pixel dc block (which was used successfully in correlators with transmissive dead-zone SLM's) is not sufficient to reduce the background-noise terms. In addition, the normalized areas of the strongly diffracting transmissive dead zones, given by  $Z_i$  in the same references, are replaced by the background transmittances  $(1 - c_1)$  or  $(1 - c_2)$ .

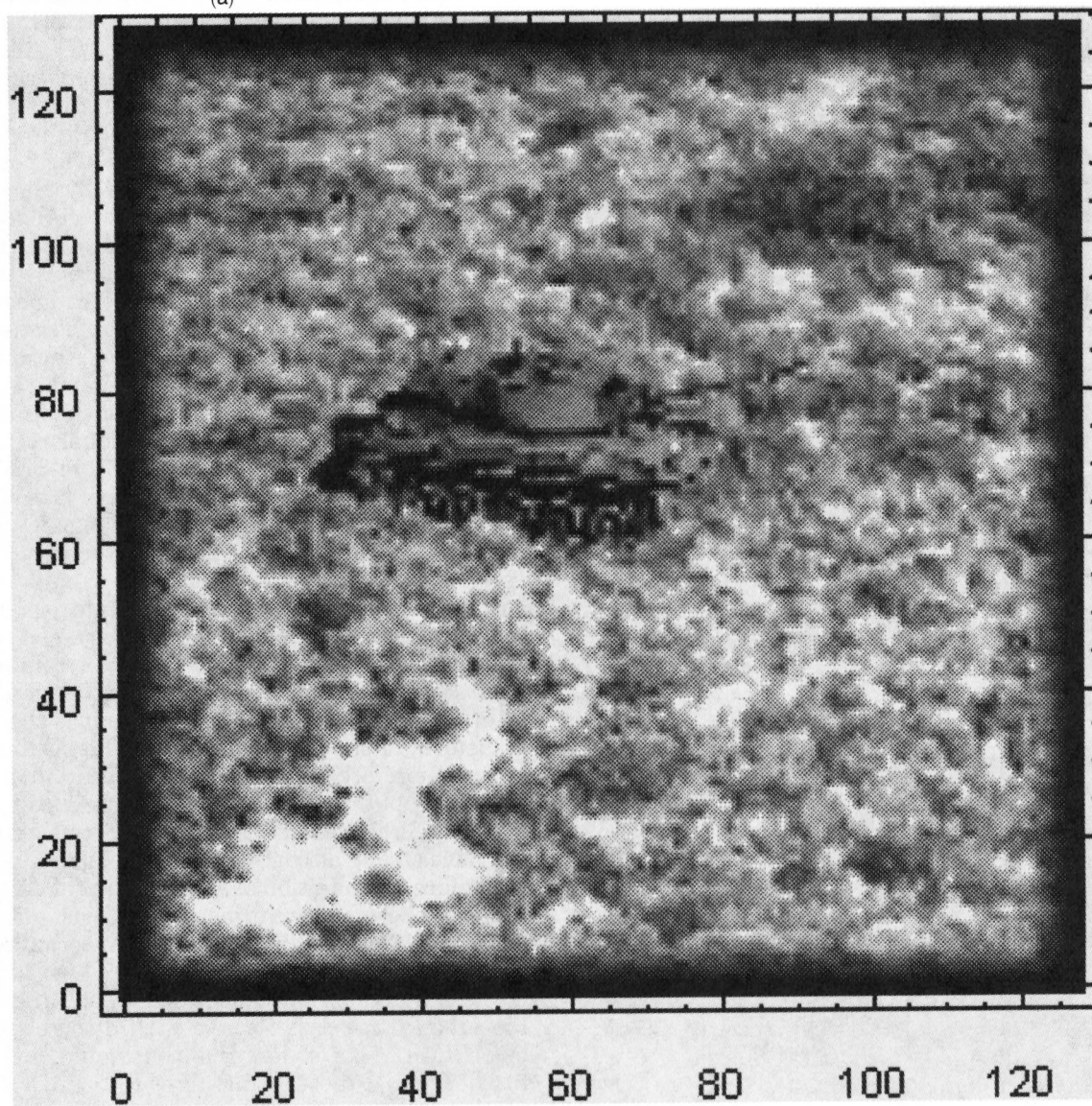
In the absence of a dc block the physical significance of the terms in relations (15)–(18) is as follows: The correlation term  $k_C$  is attenuated by the transmittances  $c_1$  of SLM1 and  $c_2$  of SLM2. The position of the correlation peak is determined by the relative locations of the signal and filter reference. The three remaining  $k$  terms [relations (16)–(18)] contribute to the background noise and coherently interfere with the  $k_C$  term. Specifically,  $k_S$  is an image of the attenuated input signal that is passed because of the finite CR of SLM2, and its position, therefore, depends on the location of the input signal. A second image,  $k_R$ , is the attenuated image of the finite CR of SLM1 (in this case, a two-dimensional rectangular image) that is passed by the finite CR of SLM2. Its positioning in the correlation plane is completely independent of the locations of the signal and filter reference. An additional distorted image,  $k_{FR}$ , is a version of  $k_R$  that is filtered by SLM2. In the correlation plane it produces a broad pattern from the blurring caused by the convolution between the rectangular image of SLM1 and the filter reference  $f^*$ . Note that  $f^*$  is an edge-enhanced version of the filter-reference input image because it is the inverse transform of the filter function. The positioning of  $k_R$  will therefore be affected by the location of  $f^*$  (the effective input image for the filter reference).

In the filter plane all three noise terms  $k_S$ ,  $k_R$ , and  $k_{FR}$  have strong dc components [see Eqs. (A9)–(A11)]. Therefore, the addition of a dc block in the filter plane reduces these noise terms, as well as noise from clutter<sup>22–24</sup> and from the convolution term occurring in  $K_c$  (Ref. 25) when a BPOF is used. Our  $3 \times 3$  pixel dc block was chosen because a  $1 \times 1$  pixel dc block lets too much noise pass for use with a correlator with low-CR SLM's. A larger block would, of course, further reduce these terms. For  $R_i > 5$ , a  $3 \times 3$  pixel block, however, keeps the ratio of the correlation peak to the second-highest peak in the correlation plane greater than 2 for the input of an uncluttered woman's face, and greater than approximately 1 for the



Fig. 3. Images that constituted the input for this study: (a) a woman's face with no background included, and (b) a tank in a noisy background.

(a)



(b)

input of a cluttered tank (see Fig. 3 below). This dc block does not, however, substantially diminish the sharp correlation peak in  $k_C$  for either the POF or BPOF.

## 6. Computer Simulations and Analysis

We performed computer simulations of this correlator and incorporated finite CR's for each SLM. Two different input images were employed. One consisted of a  $64 \times 64$  pixel array of a woman's face with no background included,<sup>1-3</sup> as shown in Fig. 3(a). This is representative of a controlled image input. Two filters were derived from this image: a phase-only filter (POF) and a binary-phase-only filter (BPOF). The other input image consisted of a  $128 \times 128$  pixel array of a tank in a desert background, as shown in Fig. 3(b). A POF and a BPOF were also derived from the tank itself, with the background removed. When all the filters were calculated, the reference image was first shifted into the middle of the upper-right quadrant of the input SLM (as was done in our previous works<sup>1-3</sup>). Our binarization axis for the BPOF was  $\zeta_0 = \pi/2$ , and approximation (9) was used to construct the filter. The input and the filter SLM's were sampled at  $2 \times 2$  points per pixel,<sup>26</sup> and the input signal was positioned at the center of a  $512 \times 512$  point zero-filled array. The correlation-intensity array in all instances was selected to be that  $128 \times 128$  point array with the correlation peak in the center.

### A. Case Studies

We analyzed three different cases for SLM's with different CR's in the input and the filter planes. These cases are listed in Table 1.

In case A the CR is the same in both SLM's (that is,  $R_1 = R_2$  and  $c_1 = c_2$ ) and varies from infinity down to 5. In this situation all four terms are present in Eq. (14), as listed in the last column of Table 1. By means of the form shown in Eq. (19),  $k_T$  can be written as

$$k_T(x_3)(\text{case A}) = c_1^2(A_C - A_S + A_R - A_{FR}) + c_1(A_S - 2A_R + A_{FR}) + A_R, \quad (20)$$

In case B the CR ( $R_2$ ) of SLM2 remains fixed at infinity ( $c_2 = 1$ ), whereas the CR's for SLM1 ( $R_1$  and  $c_1$ ) vary. As seen in relations (16) and (17),  $k_S$  and  $k_R$  vanish, leaving only  $k_C$  and  $k_{FR}$  in Eq. (14). Ex-

pressed in the form of Eq. (19),  $k_T$  can be written as

$$k_T(x_3)(\text{case B}) = c_1(A_C - A_{FR}) + A_{FR}. \quad (21)$$

In case C the CR ( $R_1$ ) of SLM1 remains fixed at infinity ( $c_1 = 1$ ), whereas the CR's for SLM2 ( $R_2$  and  $c_2$ ) vary. From relations (17) and (18),  $k_R$  and  $k_{FR}$  vanish, and  $k_T$  can be written as

$$k_T(x_3)(\text{case C}) = c_2(A_C - A_S) + A_S. \quad (22)$$

Also note that, whenever both CR's are infinite, then  $c_1 = c_2 = 1$ , so Eq. (14) reduces to the single term  $k_C$ . We see below that a dc block primarily reduces  $A_R$ ,  $A_{FR}$ , and  $A_S$ , and also, for a BPOF, the block reduces the convolution term present in  $A_C$ .

### B. Correlation Peak and Detection Metrics

The quantities computed from the resulting correlation simulations were the peak intensity ( $I_p$ ) and the metrics: peak-to-noise ratio (PNR) and peak-to-secondary ratio (PSR). These quantities are calcu-

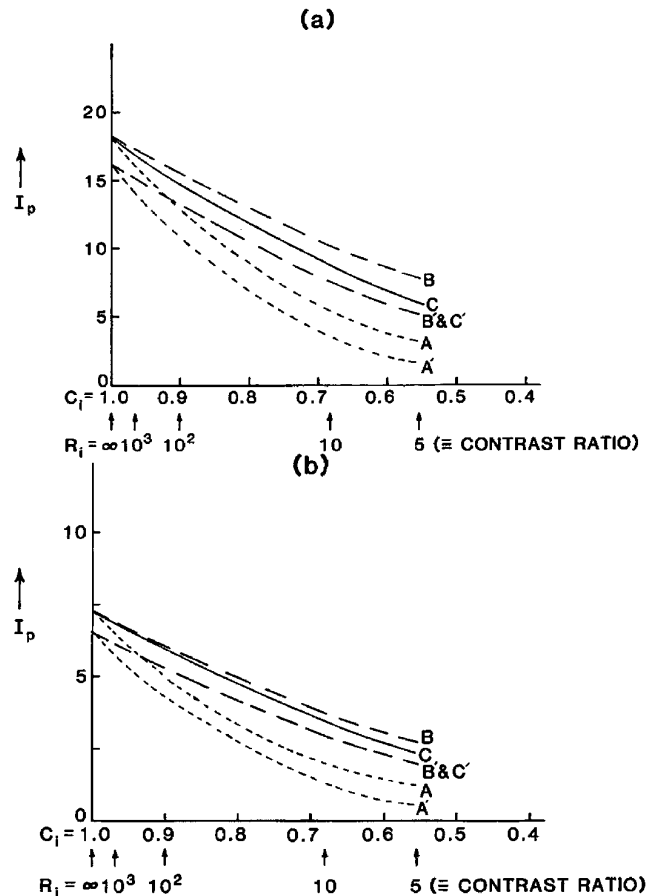


Fig. 4. Correlation peak intensity  $I_p$  versus the amplitude transmittance ( $c_i$ ) and CR ( $R_i$ ) for cases A, B, and C for (a) a POF filter, and (b) a BPOF filter that uses the woman's face. The letters without primes refer to cases in which no dc block was used, whereas the letters with primes refer to cases in which a  $3 \times 3$  pixel dc block was used in the filter plane.  $c_i$  stands for  $c_1$  for cases A, A', B and B';  $c_i$  stands for  $c_2$  for cases C and C'. Selected values of the CR,  $R_i$ , are shown below their corresponding  $c_i$ , with  $R_i \equiv R_1$  for cases A and B, and  $R_i \equiv R_2$  for case C.

Table 1. CR Case Studied

Case <sup>a</sup>	SLM1	SLM2	Nonzero $k$ Terms in $k_T$
A	$R_1$ (or $c_1$ ) varies	$R_2 = R_1$ (or $c_2 = c_1$ )	$k_C, k_S, k_R, k_{FR}$
B	$R_1$ (or $c_1$ ) varies	$R_2 = \infty$ (or $c_2 = 1$ )	$k_C, k_{FR}$
C	$R_1 = \infty$ (or $c_1 = 1$ )	$R_2$ (or $c_2$ ) varies	$k_C, k_S$

<sup>a</sup>If  $R_1 = R_2 = \infty$  for any case, then  $k_T = k_C$ .

lated as follows:

$$I_p = |k_T|_{\max}^2 \quad (23)$$

Both  $|k_T|_{\max}$  and  $|k_C|_{\max}$  occur at the same location in all instances, except for noisy inputs that are combined with low-CR SLM's. Under these latter conditions a secondary peak may be larger than the correlation peak. Next,

$$\text{PNR} = |k'|_{\max} / |k'|_{\text{SD}}, \quad (24)$$

where the subscript SD represents a standard deviation. The zero-mean array  $|k'| = |k_T| - \overline{k_T}$ , with  $\overline{k_T}$  the mean value of the entire  $|k_T|$  array and

$$|k'|_{\text{SD}} = \left[ \sum_{i \neq \max} |k_i'|^2 / (N - 1) \right]^{1/2}. \quad (25)$$

Finally,

$$\text{PSR} = |k'|_{\max} / |k'|_{\text{(highest secondary peak)}}. \quad (26)$$

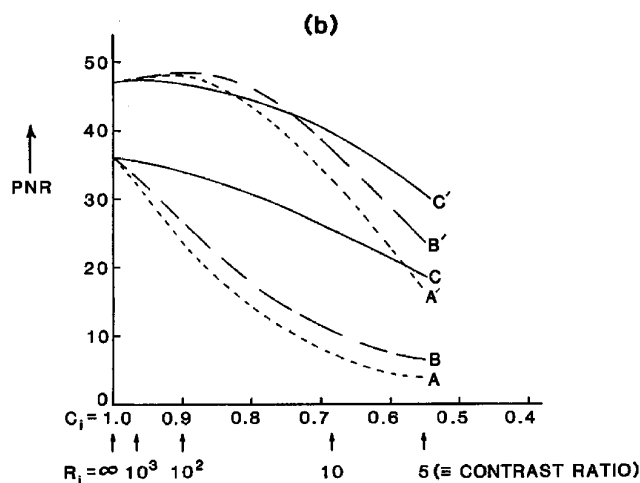
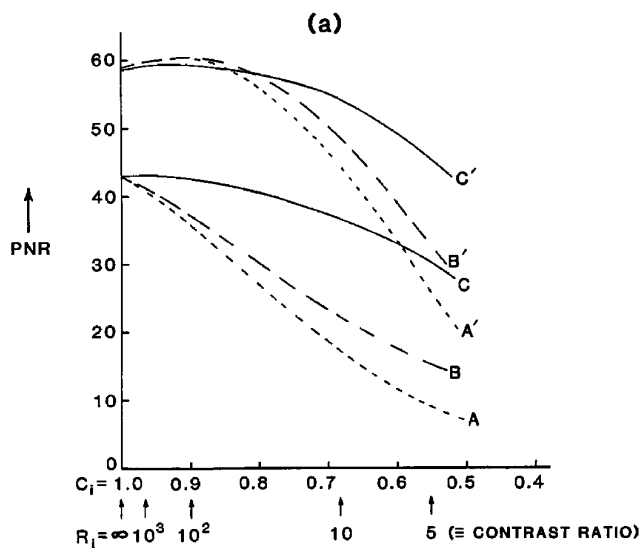


Fig. 5. Same as in Figs. 4(a) and (b), except that the ordinate is the peak-to-noise ratio (PNR).

### C. Correlation-Peak Intensity Simulations for Input of the Woman's Face

In one part of this study a woman's face, shown in Fig. 3(a), was used for both the input and the filter. Figure 4 shows how the computer-calculated correlation-peak intensity  $I_p$  changes with the transmittance coefficient  $c_i$  for the three cases listed in Table 1. In Fig. 4(a) a POF is used as the filter and in Fig. 4(b) a BPOF is used. As discussed in Section 6.B.,  $c_i \equiv c_1$  for cases A and B; whereas,  $c_i \equiv c_2$  for case C. Some values of the contrast ratio  $R_i$  are shown below their corresponding  $c_i$ . Note that for a constant  $c_i$  and no dc block, regardless of the type of filter used, case B gives a higher  $I_p$  value than case C because of the addition of more noise to the correlation background. Meanwhile, case A gives the lowest  $I_p$  because it

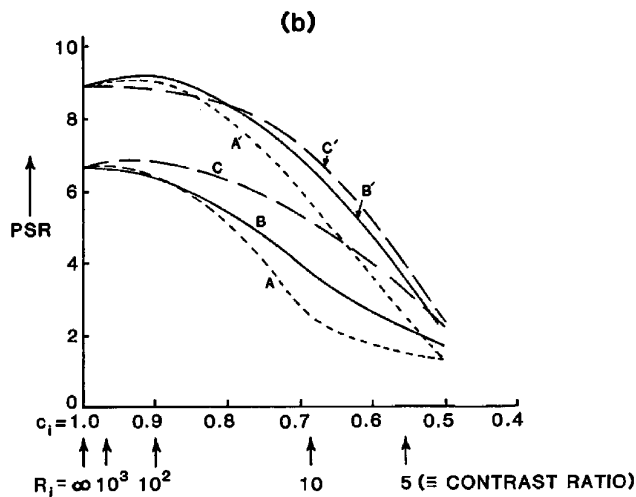
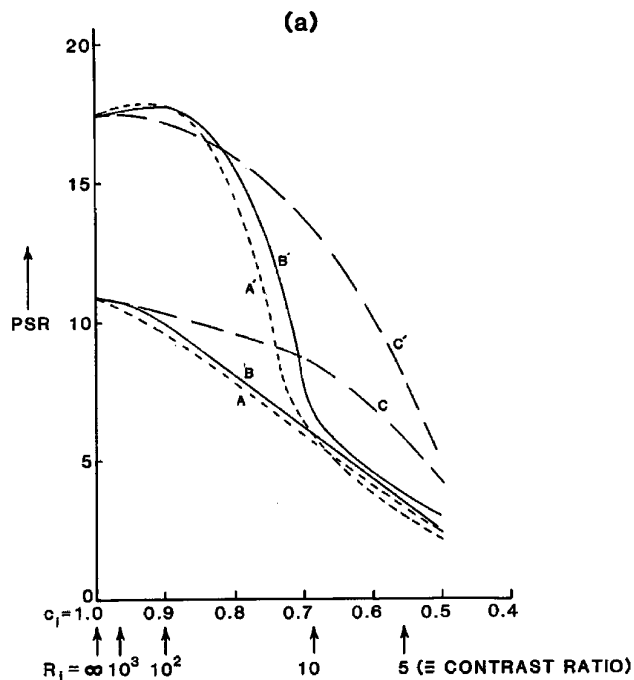


Fig. 6. Same as in Figs. 4(a) and (b), except the ordinate is peak-to-sidelobe ratio (PSR).

combines the losses of signals associated with cases B and C.

With the insertion of a  $3 \times 3$  pixel dc block all three curves (now indicated by primes) are depressed, and the curves for cases B' and C' are close enough to be superimposed. In this circumstance and at a value of  $c_i = 1$  (that is, perfect SLM's), the magnitude of  $I_p$  with either filter drops to approximately 85% of its unblocked value. With the dc block still included and at a  $c_i$  of 0.553 ( $R_i = 5$ ),  $I_p$  for either filter drops to approximately 31% of its value at  $c_i = 1$  for cases B' and C' and to approximately 9% for case A'.

The falloff of  $I_p$  with  $c_i$  is quantitatively proportional to  $c_i^4$  for case A' and to  $c_i^2$  for cases B' and C'. For a  $3 \times 3$  pixel dc block this reduction in  $I_p$  as the CR decreases agrees well with Eqs. (20)–(22) for both filters because most of the noise terms are removed. For example, for  $R_i = 5$  the agreement of the simulation results with the theory is within  $\pm 6\%$ . With no dc block the peak intensities for cases A, B, and C have a stronger noise background and do not fall off as rapidly as the theory for the correlation peak predicts.

When dc blocks are added, the falloff of the intensities in Fig. 4 is algebraically similar to that reported in Refs. 1–3. In dead-zone correlators a substantial amount of energy never reaches the detector. It is lost through the strong higher-order diffraction from the dead zones of the two SLM's and only a 1-pixel dc block is required for  $I_p$  to agree with the theory. For the same correlation-peak signal  $(k_C)_{\text{peak}}$  in finite-CR correlators, much less energy is lost to higher-order diffraction, as is discussed in Section 6.H. Consequently, a  $3 \times 3$  pixel dc block is now required to reduce this excess noise in the correlation plane.

#### D. PNR and PSR Results for the Input Consisting of a Woman's Face

The PNR and PSR results for the POF and BPOF were calculated as a function of transmittance coefficient  $c_i$ . The results for these metrics, in which the woman's face was used as input, are shown in Figs. 5(a) and 6(a) for the POF, and in Figs. 5(b) and 6(b) for the BPOF. The unprimed cases indicate operation with no dc block; the primed cases indicate operation with a  $3 \times 3$  pixel dc block.

For both filters, Figs. 5 and 6 show that there is a falloff in the PNR and the PSR as  $c_i$  decreases. For cases A and B the PNR falloff is rapid, indicating strong noise contributions. The actual values for case A are the smallest (just as in the transmissive dead-zone correlator) because this case combines the noise of cases B and C. For case C the PNR falls off much more slowly than in the other two cases because the signal converted to noise that is due to the CR of the filter SLM is relatively small. In fact, the PNR's for this case remain nearly constant until  $c_2 < 0.85$ .

With the addition of the  $3 \times 3$  pixel, opaque dc block, Figs. 5 and 6 show how much the performance values are improved. Some of the actual values for these performance metrics and their improvement factors are listed in the upper half of Table 2. For example, at  $c_i = 1$ , the PNR and the PSR improve by factors of from 1.3 to 1.6, respectively. At  $c_i = 0.553$  ( $R_i = 5$ ), the PNR's for both filters improve by factors ranging from 1.5 to 4.9; whereas the PSR's improve marginally for the POF and only slightly for the BPOF. An explanation of the columns in Table 2 that are labeled "Gray dcB" (where dcB represents dc block) are given in Section 6.G.

Table 2. Operating Values of Various Metrics when a  $3 \times 3$  Pixel dc Block Is Added to Filter SLM<sup>a</sup>

Input	Filter	Case	$R$	Improvement Factors						
				Opaque dcB Operation			PNR		PSR	
				PNR	PSR	$I_p$	Opaque dcB	Gray dcB	Opaque dcB	Gray dcB
Woman's face	POF	All	$\infty$	59.2	17.4	16.3	1.4	1.3	1.6	1.4
		A	5	26.2	3.0	1.6	2.9	1.6	0.91	0.70
		B	5	33.0	3.8	5.1	2.1	1.5	1.1	1.0
		C	5	45.6	7.9	5.2	1.5	1.3	1.4	1.2
	BPOF	All	$\infty$	47.3	9.0	6.5	1.3	1.2	1.3	1.3
		A	5	17.0	2.6	0.6	4.9	2.0	1.7	1.5
		B	5	23.8	3.6	2.0	3.7	1.9	1.6	1.6
		C	5	31.0	4.0	2.1	1.5	1.3	1.2	1.1
Tank	POF	All	$\infty$	15.6	3.4	1.7	1.8	1.1	1.2	0.9
		A	5	6.5	1.4	0.16	1.9	0.8	1.0	0.8
		B	5	5.8	1.2	0.41	1.3	0.8	0.7	0.6
		C	5	15.0	3.4	0.55	2.4	1.0	1.6	0.9
	BPOF	All	$\infty$	9.9	2.3	0.71	2.4	1.6	2.3	1.5
		A	5	4.8	1.2	0.83			[1.7]	[1.2]
		B	5		0.8	0.17			[1.4]	[1.2]
		C	5	10.3	1.2	0.83			[2.4]	[1.4]

<sup>a</sup>Square brackets indicate values for which the correlation peak was not at the maximum. Blank entries indicate that measurements are not possible under those circumstances.

### E. Performance Simulation with the Tank Input

The tank input, shown in Fig. 3(b), introduces substantially more noise to the correlation signal than does the clutter-free face input. Clutter makes both dc and spatial frequency-dependent contributions to the noise at the filter, but the high-frequency portion cannot be removed with a dc block. Moreover, a large clutter value combined with a low CR can have the effect of elevating a secondary peak higher than the correlation peak, thus causing the PSR to be less than unity. In addition, the noise level is high enough so that the theoretically predicted falloffs of  $I_P$  are not achieved.

With the insertion of the  $3 \times 3$  pixel, opaque dc block and for an infinite CR, the correlation intensities at the usual peak position are reduced by 40% and 35% for the POF and BPOF, respectively. These values are listed in the lower half of the Table 2. They are lower than the corresponding values for the face input by factors of 9.8 and 9.2, respectively. Some of the reasons why this occurs is that a portion of the clutter is brighter than the tank, and the maximum value of the tank input is normalized to unity for SLM1. Also, as indicated in Fig. 3, the tank is smaller in size than the woman's face.

The actual values of the PNR, the PSR, and the  $I_P$  for the POF and BPOF with this dc block when the input signal is the cluttered tank are shown in Table 2. No PNR value is shown for the BPOF for case B because the PSR is still less than unity.

The lower half of Table 2 also shows that, for the POF, the PNR's improve by factors of 1.3 to 2.4, whereas the PSR's improve only marginally. For  $R_i \rightarrow \infty$  these PNR's are factors of 3.8 and 4.8 less than the corresponding POF and BPOF values, respectively, for the input of the woman's face. For the BPOF, when  $R_i < \infty$  the correlation peak is not the maximum peak in the correlation pattern, so the PNR's are not evaluated, as is indicated by the brackets in Table 2, and the PSR's are all less than unity. It is only with the insertion of the dc block that the PSR's rise above unity, rendering the BPOF correlator useable again. The improvement factors in the PSR's are indicated within such brackets.

### F. Opaque dc Block

A  $3 \times 3$  pixel, opaque dc block has been shown to improve the PNR and the PSR and to produce a closer agreement with both the  $c_i$  falloff value predicted for  $I_P$  from Eq. (20) and the flat  $c_i$  dependence for  $c_i > 0.85$  observed for the PNR and the PSR.

One example that vividly demonstrates the effect of the  $3 \times 3$  pixel dc block is shown in Fig. 7. In Fig. 7(a) we see the three-dimensional correlation pattern for a correlator employing the woman's face. Both of the correlator's SLM's have a CR of 5 (case A), and its filter is a BPOF with no dc block. The PNR and the PSR are 3.7 and 1.5, respectively. The detector has been positioned so that the correlation peak  $k_C$  is located at its center. The bumpy portion in the far-right quadrant is the woman's image  $k_S$ .  $k_C$  and

$k_S$  sit on top of the rectangular platform  $k_R$ . The attenuated skirt around this platform is made up of the  $k_{FR}$  and the convolution portion of the  $k_C$  that was introduced by the BPOF. When a  $3 \times 3$  pixel, opaque dc block is inserted at the center of SLM2, there is noise reduction in  $k_S$ ,  $k_R$ , and  $k_{FR}$ , and the extent of this reduction is clearly demonstrated in Fig. 7(b). For the situation shown here, the PNR increases to 17.0 and the PSR to 2.6.

### G. Gray dc Block

Because a perfectly opaque dc block may be difficult to realize in fabrication, we simulated the performance of a partially attenuating (that is, gray)  $3 \times 3$  pixel dc block in SLM2. This is what would be obtained from

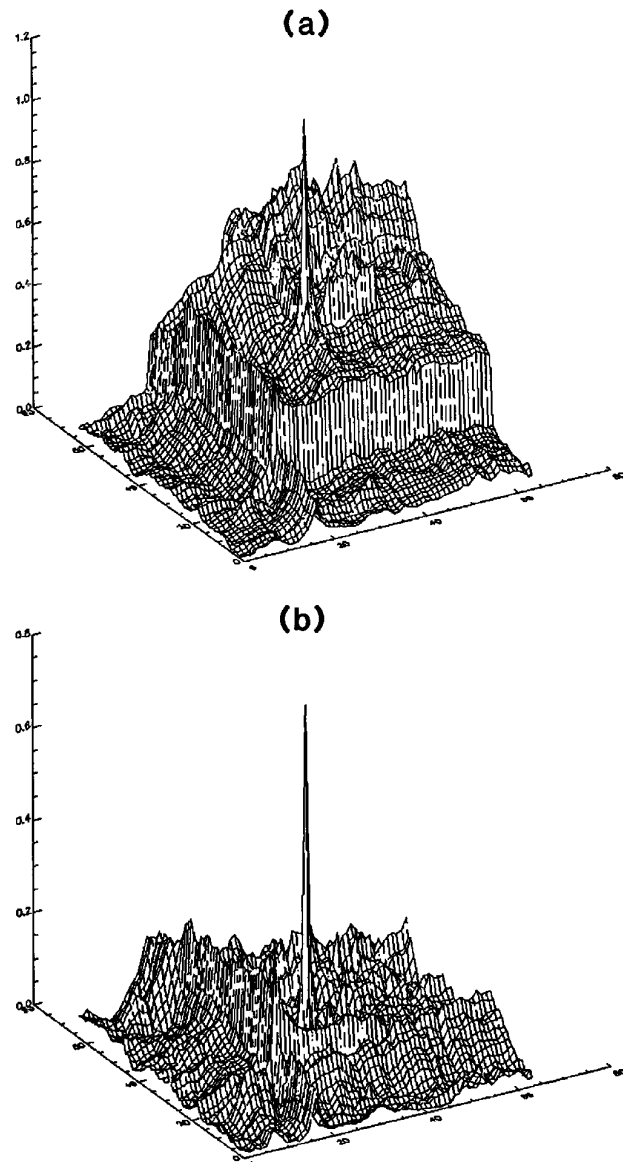


Fig. 7. Three-dimensional correlation patterns for a correlator whose SLM's each have CR = 5 (case A) and in which the filter SLM contains a binary-phase-only filter (a) with no dc block and (b) with a  $3 \times 3$  pixel dc block in the filter plane. The woman's face was used for both the input and the filter.

**Table 3. Energy Partitioning in Percent throughout the Correlator with and without the Use of a dc Block for the Input of the Woman's Face**

Filter Type and Case	dc Block Used	Contrast Ratio $R_i$	Light Missing the Filter	Light Eliminated by the dc Block	Light Loss from the Phase-Only Filter <sup>a</sup>	Light Missing the Detector	Light Recorded by the Detector <sup>b</sup>
POF							
All	Yes	$\infty$	2.3	48.0	0	13.8	35.9
	No	$\infty$	2.3	0	0	26.3	71.4
A	Yes	5	0.2	87.7	5.5	3.8	2.8
	No	5	0.2	0	24.4	24.3	51.1
B	Yes	5	0.2	87.7	0	6.9	5.2
	No	5	0.2	0	0	34.6	65.2
C	Yes	5	2.3	48.0	41.5	5.1	20.4
	No	5	2.3	0	41.5	8.0	48.2
BPOF							
All	Yes	$\infty$	2.3	48.0	0	20.2	29.5
	No	$\infty$	2.3	0	0	38.0	59.7
A	Yes	5	0.2	87.7	5.3	4.2	2.6
	No	5	0.2	0	8.1	31.9	59.8
B	Yes	5	0.2	87.7	0	7.7	4.4
	No	5	0.2	0	0	36.9	62.9
C	Yes	5	2.3	48.0	24.3	5.0	20.4
	No	5	2.3	0	33.8	11.6	52.3

<sup>a</sup>This light loss occurs for all phases of  $F^*$  that are different from zero.

<sup>b</sup>This light loss occurs because SLM2 diffracts the incident light at too large an angle to permit it to be captured at the detector.

an amplitude-modulated SLM if we electrically turned off the center  $3 \times 3$  pixels. For an SLM with our minimum CR of 5, the corresponding intensity transmittance would be 20%. In columns 9 (gray dcB values of the PNR) and 11 (gray dcB values of the PSR) in Table 2 we list the improvement factors in the two metrics caused by this gray dc block. Note that for the case of the input of the woman's face the improvement factors for the PNR now extend only from 1.2 to 2.0, whereas before they went from 1.3 to 4.9. The PSR factors did not change much. For

the tank input, the insertion of the gray dc block actually worsened the two performance metrics.

#### H. Energy Budget

The energy partitioning for correlators that have SLM's with CR's of  $\infty$  and 5 are listed in Table 3 for the input of the woman's face and in Table 4 for the input of the tank. Entries are stated in a percentage of the total light exiting from SLM1. When these numbers are compared with those in a similar table (Table 4) in Ref. 2, they indicate the differences

**Table 4. Energy Partitioning in Percent throughout the Correlator with and without the Use of a dc Block for the Input of the Tank**

Filter Type and Case	dc Block Used	Contrast Ratio $R_i$	Light Missing the Filter	Light Eliminated by the dc Block	Light Loss from the Phase-Only Filter <sup>a</sup>	Light Missing the Detector	Light Recorded by the Detector <sup>b</sup>
POF							
All	Yes	$\infty$	0.5	83.3	0	8.4	7.8
	No	$\infty$	0.5	0	0	36.1	63.4
A	Yes	5	0.1	87.0	8.1	2.7	2.1
	No	5	0.1	0	32.5	23.4	44.0
B	Yes	5	0.1	87.0	0	7.0	5.9
	No	5	0.1	0	0	35.9	64.0
C	Yes	5	0.5	83.3	9.9	3.3	3.0
	No	5	0.5	0	33.3	23.6	42.6
BPOF							
All	Yes	$\infty$	0.5	83.3	0	8.4	7.8
	No	$\infty$	0.5	0	0	41.8	57.7
A	Yes	5	0.1	87.0	8.2	2.9	1.8
	No	5	0.1	0	16.8	30.6	52.5
B	Yes	5	0.1	87.0	0	7.7	5.2
	No	5	0.1	0	0	41.1	58.8
C	Yes	5	0.5	83.3	10.0	3.8	2.4
	No	5	0.5	0	18.7	30.8	50.0

<sup>a</sup>This light loss occurs for all phases of  $F^*$  that are different from zero.

<sup>b</sup>This light loss occurs because SLM2 diffracts the incident light at too large an angle to permit it to be captured at the detector.

between correlators fabricated with SLM's that have finite CR's and those with transparent dead zones. The values in Tables 3 and 4 pertain to the situation when a  $3 \times 3$  pixel, opaque dc block is or is not applied to SLM2. Columns 4 through 8 refer to the following, respectively: light that misses the filter because it was diffracted at too large an angle by SLM1, additional light eliminated by the dc block itself, light loss associated with the phase-only filter (occurring for all phases of  $F^*$  different from zero), light that misses the detector because SLM2 diffracts it at too large an angle, and light recorded by the detector. The values across any row always add to 100%.

Our simulations show that much more energy exits SLM1 when its CR is finite than when it is infinite. This is due to the additional energy that is allowed to pass through the pixels from the signal illuminating SLM1. For example, when the image of the woman's face is used as input, the energy exiting SLM1 when it has a CR of 5 is 11 times greater than when SLM1 has an infinite CR, and the percentage of this energy that is a true signal would be only 2.8%. On the other hand, when the image of the tank is used as input, the energy exiting SLM1 when it has a CR of 5 is only 1.7 times greater than when SLM1 has an infinite CR, but only 18% of that represents the true signal. (We note that there is 13.6 times more energy in the tank-scene input than in the facial-scene input.

## 7. Conclusions and Recommendations

We have presented an analytical model and computer simulations for the performance of optical correlators with SLM's that have varying CR's by using two gray-scale real-world images: a tank in nonoverlapping clutter and a woman's face. Furthermore, we have shown that this analytical model and the computer simulations are in agreement. Our analytical results revealed that when SLM's in correlators have finite CR's the total correlation pattern consists of four parts: one gives the true correlation and the other three form background noise.

As a result of our study we arrive at the following conclusions for SLM's that have CR's as low as 5:

(1) Correlation performance in the form of the PNR, the PSR, and the peak intensity  $I_p$  is always better when a POF, rather than a BPOF, is used in the system.

(2) Insertion of a dc block at the center of the filter SLM decreases the background noise in the correlation plane; this dc block is larger than that required for the same level of performance in a correlator whose SLM's have transmissive (or reflective) dead zones.

(3) For both cluttered and uncluttered input, regardless of the type of phase filter used and with an opaque dc block inserted, this study indicates that the three metrics of  $I_p$ , PNR, and PSR are usually highest for case C (the input SLM is perfect) and lowest for case A (both SLM's have a finite CR).

These computer simulations and the analytical model demonstrate that as the CR's of the SLM's are lowered the following occurs: the correlation peaks decrease, the background noise increases, and consequently the performance measures diminish. Nonetheless, for our two substantially different input types, we have shown that, even with CR's as low as 5, correlators employing either a POF or a BPOF can still perform quite satisfactorily (1) with or without a dc block for either type of filter if the input scene is noise and clutter free, and (2) only with a dc block when a BPOF is used if the input scene is significantly cluttered. Finally, we recommend that the user place the SLM with the highest CR in the input plane and use a dc block in the filter plane.

## Appendix A.

The analysis presented here is similar to that presented in Ref. 3 for the case of pixellated SLM's that have transmissive (or reflective) dead zones. We have kept the same symbols for similar terms. In the notation of this paper all terms that have a subscript 1 refer to the input plane, those that have a subscript 2 to the filter plane, and those that have a subscript 3 to the output plane. For notational simplicity we present a one-dimensional signal analysis that may be directly extended to two dimensions.

Because the continuous (and normalized) incident signal  $s(x_1)$  in Fig. 1 is detected, sampled, and addressed to discrete pixels in SLM1, Eq. (4) from the text must be modified accordingly. The complete expression for  $w(x_1)$  becomes

$$w(x_1) = \left[ c_1 \left[ \sum_{n=-\infty}^{\infty} [\delta(x_1 - nb_1)] s(x_1) \right] \circ \text{rect} \left( \frac{x_1}{b_1} \right) + (1 - c_1) \text{rect} \left( \frac{x_1}{L_1} \right) \right]. \quad (\text{A1})$$

Here,  $s$  addresses pixels of width  $b_1$  and the convolution operation with  $\text{rect}(x_1/b_1)$  maintains that sampled value across the pixel face. The  $\text{rect}(x_1/L_1)$  term accounts for the length  $L_1$  of SLM1. The effects of the transfer characteristic and the finiteness of the CR are reflected in term  $c_1$ . A Fourier transformation yields

$$W(\xi_2) = \left( c_1 \left[ \sum_{n=-\infty}^{\infty} \delta \left( \xi_2 - \frac{n}{b_1} \right) \circ S(\xi_2) \right] \text{sinc}(b_1 \xi_2) \right) + (1 - c_1) \delta(\xi_2) \circ L_1 \text{sinc}(L_1 \xi_2), \quad (\text{A2})$$

where  $S(\xi_2)$  is the Fourier transform of  $s(x_1)$ . Only the  $n = 0$  term need be kept because the higher-order terms are centered at positions beyond the edges of the filter and make negligible contributions within the confines of the filter.

In a similar manner the basic portion of  $G^*(\xi_2)$  [see Eq. (9)] has to be modified to include the discreteness of the pixels in SLM2. For illumination by a unit-

amplitude plane wave, the output from SLM2 is given by

$$G^*(\xi_2) = \left[ c_2 \left( \sum_{m=-\infty}^{\infty} \delta[\xi_2 - m(\Delta\xi_2)] F^*(\xi_2) \right) \circ \text{rect}(L_1\xi_2) + (1 - c_2) \right] \text{rect}\left(\frac{x_2}{L_2}\right), \quad (\text{A3})$$

where  $\Delta\xi_2$  gives the width of SLM2's pixels in spatial-frequency coordinates and  $\text{rect}(x_2/L_2)$  accounts for the length  $L_2$  of SLM2. Also, if a dc block consisting of  $p_2$  pixels along each dimension, each pixel having a width  $h_2$ , is placed at the center of SLM2, then the term  $\text{rect}(x_2/L_2)$  in Eq. (A3) would be replaced by

$$\text{rect}\left(\frac{x_2}{L_2}\right) - \text{rect}\left(\frac{x_2}{p_2h_2}\right) \equiv T_{\text{dc}}(x_2). \quad (\text{A4})$$

The relation between spatial coordinates ( $x_2$ ) and spatial-frequency coordinates ( $\xi_2$ ) in the filter plane, which maintains the minimum resolving power in that plane, is given by  $x_2 = L_1h_2\xi_2$ . Consequently,  $\Delta\xi_2$  in Eq. (A3) can be replaced by  $1/L_1$ ;  $x_2/L_2$  can be replaced by  $L_1h_2\xi_2/L_2$ , and  $x_2/p_2h_2$  can be replaced by  $L_1\xi_2/p_2$ . Thus, the spatial-frequency form of Eq. (A3) can be written as

$$G^*(\xi_2) = \left[ c_2 \left( \sum_{m=-\infty}^{\infty} \delta\left(\xi_2 - \frac{m}{L_1}\right) F^*(\xi_2) \right) \circ \text{rect}(L_1\xi_2) + (1 - c_2) \right] T_{\text{dc}}(\xi_2), \quad (\text{A5})$$

where

$$T_{\text{dc}}(\xi_2) = \text{rect}\left(\frac{L_1h_2\xi_2}{L_2}\right) - \text{rect}\left(\frac{L_1\xi_2}{p_2}\right). \quad (\text{A6})$$

The output from SLM2 is given by the function  $K_T(\xi_2)$ , which consists of the product  $|W(\xi_2)|G^*(\xi_2)$ . From Eqs. (A2) and (A5),  $K_T(\xi_2)$  can be written as the sum of the four terms:

$$K_T(\xi_2) = K_C(\xi_2) + K_S(\xi_2) + K_R(\xi_2) + K_{FR}(\xi_2), \quad (\text{A7})$$

in which the meaning behind the subscripts is given in the text. Specifically,

$$K_C(\xi_2) = (c_1c_2)[S(\xi_2)]\text{sinc}(b_1\xi_2) \circ L_1 \text{sinc}(L_1\xi_2) \times \left( \sum_{m=-\infty}^{\infty} \delta\left(\xi_2 - \frac{m}{L_1}\right) F^*(\xi_2) \right) \circ \text{rect}(L_1\xi_2) T_{\text{dc}}(\xi_2), \quad (\text{A8})$$

$$K_S(\xi_2) = [c_1(1 - c_2)]S(\xi_2)\text{sinc}(b_1\xi_2) \circ L_1 \text{sinc}(L_1\xi_2) T_{\text{dc}}(\xi_2), \quad (\text{A9})$$

$$K_R(\xi_2) = (1 - c_1)(1 - c_2)[\delta(\xi_2) \circ L_1 \text{sinc}(L_1\xi_2)] T_{\text{dc}}(\xi_2), \quad (\text{A10})$$

and

$$K_{FR}(\xi_2) = (1 - c_1)c_2[\delta(\xi_2) \circ L_1 \text{sinc}(L_1\xi_2)] \times \left( \sum_{m=-\infty}^{\infty} \delta\left(\xi_2 - \frac{m}{L_1}\right) F^*(\xi_2) \right) \circ \text{rect}(L_1\xi_2) \times T_{\text{dc}}(\xi_2), \quad (\text{A11})$$

When the above  $K$  terms are inverse transformed they result in the following four correlation terms, where  $x_3$  is the spatial coordinate in the output plane:

$$k_C(x_3) = \left[ c_1c_2 \left[ s(x_3) \circ \text{rect}\left(\frac{x_3}{b_1}\right) \right] \text{rect}\left(\frac{x_3}{L_1}\right) \right] \star \left[ \sum_{m=-\infty}^{\infty} \delta(x_3 - mL_1) \star f^*(x_3) \right] \times \text{sinc}\left(\frac{x_3}{L_1}\right) \circ t_{\text{dc}}(x_3), \quad (\text{A12})$$

in which  $f^*(x_3)$  is the impulse response of  $F^*(\xi_2)$ , the star represents correlation, the detector length is  $L_1$ , and  $t_{\text{dc}}(x_3)$  is given by Eq. (13) in Section 4. In the term involving  $f^*(x_3)$  we select the  $m = 0$  term only, assuming other values of  $m$  will cause  $f^*(x_3 - mL_1)$  to fall outside of the detector. Apart from the  $t_{\text{dc}}(x_3)$  and the  $c_1c_2$  terms, the rest of the expression in Eq. (A12) represents the usual correlation term that occurs when  $c_1 = c_2 = 1$ . Continuing,

$$k_S(x_3) = \left[ c_1(1 - c_2) \left[ s(x_3) \circ \text{rect}\left(\frac{x_3}{b_1}\right) \right] \text{rect}\left(\frac{x_3}{L_1}\right) \right] \circ t_{\text{dc}}(x_3), \quad (\text{A13})$$

$$k_R(x_3) = (1 - c_1)(1 - c_2) \text{rect}\left(\frac{x_3}{L_1}\right) \circ t_{\text{dc}}(x_3), \quad (\text{A14})$$

$$k_{FR}(x_3) = (1 - c_1)c_2 \left[ \text{rect}\left(\frac{x_3}{L_1}\right) \star \left[ f^*(x_3) \cdot \text{sinc}\left(\frac{x_3}{L_1}\right) \right] \right] \circ t_{\text{dc}}(x_3), \quad (\text{A15})$$

In Eqs. (A12)–(A15) the dc-blocking term  $t_{\text{dc}}$ , which also plays the role of a blurring function, can be rewritten to take into consideration the transmittance (or grayness) of the block. If this grayness is included, Eq. (A6) can be recast as

$$T_{\text{dc}}(\xi_2) = \text{rect}\left(\frac{L_1h_2\xi_2}{L_2}\right) \left[ 1 - (1 - \epsilon) \text{rect}\left(\frac{L_2\xi_2}{p_2}\right) \right], \quad (\text{A16})$$

where  $\epsilon$  is the amplitude transmittance of the dc block, that is, when  $\epsilon$  is zero the block is opaque, whereas when  $\epsilon$  is unity the block is completely transmissive. Note that factoring out the term representing the wider rectangular function does not

affect the narrow rectangular function inside the bracket. The Fourier transform of Eq. (A16) is

$$t_{dc}(x_3) = \frac{L_2}{L_1 h_2} \text{sinc}\left(\frac{L_2 x_3}{L_1 h_2}\right) \circ \left[ \delta(x_3) - (1 - \epsilon) \frac{p_2}{L_1} \text{sinc}\left(\frac{p_2}{L_1} x_3\right) \right], \quad (\text{A17})$$

With this expression the final  $k_T$  can be expressed as

$$k_T(x_3) = [k_T(x_3)]_{p_2=0} - (1 - \epsilon) [k_T(x_3)]_{p_2=0} \circ \frac{p_2}{L_1} \text{sinc}\left(\frac{p_2}{L_1} x_3\right). \quad (\text{A18})$$

The second term subtracts a low-pass amplitude term from  $k_T$ . For example, the correlation peak  $k_C$  is large for POF correlators, and our simulations with perfect SLM's yield a 6% reduction in the peak amplitude for a  $3 \times 3$  pixel dc block. The broad noise components in  $k_R$ ,  $k_S$ , and  $k_{FR}$  are, however, strongly reduced, as indicated by the increase in the PNR shown in Figs. 5(a) and 5(b). In Fig. 5(b) the BPOF convolution term has also been reduced.<sup>25</sup>

The authors would like to acknowledge David Flannery for informative discussions.

## References and Notes

1. P. D. Gianino and C. L. Woods, "Effects of spatial light modulator opaque dead zones on optical correlation," *Appl. Opt.* **31**, 4025–4033 (1992).
2. P. D. Gianino and C. L. Woods, "General treatment of spatial light modulator dead-zone effects on optical correlation. I. Computer simulations," *Appl. Opt.* **32**, 6527–6535 (1993).
3. P. D. Gianino and C. L. Woods, "General treatment of spatial light modulator dead-zone effects on optical correlation. II. Mathematical analysis," *Appl. Opt.* **32**, 6536–6541 (1993).
4. C. Warde and A. D. Fisher, "Spatial light modulators: applications and functional capabilities," in *Optical Signal Processing*, J. L. Horner, ed. (Academic, New York, 1987), pp. 507–508.
5. R. M. Turner, D. A. Jared, G. D. Sharp, and K. M. Johnson, "Optical correlator using very-large-scale integrated circuit ferroelectric-liquid crystal electrically addressed spatial light modulators," *Appl. Opt.* **32**, 3094–3101 (1993).
6. K. M. Johnson, D. A. Jared, T. Slagle, K. Wanger, C. Mao, and M. G. Robinson, "Ferroelectric liquid crystal spatial light modulators and their applications," in *Spatial Light Modulators and Applications*, Vol. 14 of OSA Technical Digest Series (Optical Society of America, Washington, D.C., 1990), pp. 90–93.
7. J. A. Davis, J. Gamlieli, and G. W. Bach, "Optical transmission and contrast ratio studies of the magneto-optic spatial light modulator," *Appl. Opt.* **27**, 5194–5201 (1988).
8. J. A. Davis and J. M. Waas, "Current status of the magneto-optical spatial light modulator," in *Spatial Light Modulators and Applications III*, U. Efron, ed., *Proc. Soc. Photo-Opt. Instrum. Eng.* **1150**, 27–43 (1989).
9. N. F. Hartman and T. K. Gaylord, "Coherent optical characterization of magneto-optical spatial light modulators," *Appl. Opt.* **29**, 4372–4383 (1990).
10. J. A. Davis and M. A. Waring, "Contrast ratio improvement for the two-dimensional magneto-optic spatial light modulator," *Appl. Opt.* **31**, 6183–6184 (1992).
11. J. L. Horner and P. D. Gianino, "Signal-dependent phase distortion in optical correlators," *Appl. Opt.* **26**, 2484–2490 (1987).
12. R. D. Juday, "Optical realizable filters and the minimum Euclidean distance principle," *Appl. Opt.* **32**, 5100–5111 (1993).
13. S. E. Monroe, C. Soutar, and R. D. Juday, "Laboratory implementation of optimal filter algorithms for copuled spatial light modulators," in *Optical Pattern Recognition IV*, D. P. Casasent, ed., *Proc. Soc. Photo-Opt. Instrum. Eng.* **1959**, 278–283 (1993).
14. R. W. Cohn and J. L. Horner, "Effects of systematic errors on phase-only correlation," *Appl. Opt.* **33**, 5432–5439 (1994).
15. M. A. Flavin and J. A. Horner, "Amplitude encoded phase-only filters," *Appl. Opt.* **28**, 1692–1696 (1989).
16. W. S. Ewing, "Silicide mosaic array compensation" in *Technical Issues in Infrared Detectors and Arrays*, E. Krikorian, ed., *Proc. Soc. Photo-Opt. Instrum. Eng.* **409**, 102–106 (1983).
17. J. M. Mooney, F. D. Shepherd, W. S. Ewing, J. E. Murguia, and J. Silverman, "Responsivity nonuniformity limited performance of infrared staring cameras," *Opt. Eng.* **28**, 1151–1161 (1989).
18. J. Silverman, J. M. Mooney, and F. D. Shepherd, "Infrared video cameras," *Sci. Am.* **266**, 78–83 (1992).
19. U. Mahlab, J. Shamir, and H. J. Caulfield, "Genetic algorithm for optical pattern recognition," *Opt. Lett.* **16**, 648–650 (1991).
20. J. Khoury, J. Fu, M. Cronin-Golomb, and C. L. Woods, "Quadratic processing and nonlinear optical phase rectification in noise reduction," *J. Opt. Soc. Am. B* **11**, 1960–1971 (1994); J. Fu, J. Khoury, M. Cronin-Golomb, and C. L. Woods, "Photorefractive two-beam coupling optimal thresholding filter for additive signal-dependent noise reduction," *Appl. Opt.* **34**, 346–351 (1995).
21. R. W. Cohn and J. L. Horner, "Performance models of correlators with random and systematic phase errors," in *Advances in Optical Information Processing VI*, D. R. Pape, ed., *Proc. Soc. Photo-Opt. Instrum. Eng.* **2240**, 270–277 (1994).
22. D. L. Flannery, J. S. Loomis, and M. E. Milkovich, "Transform-ratio ternary phase-amplitude filter formulation for improved correlation discrimination," *Appl. Opt.* **27**, 4079–4083 (1988).
23. K. Fielding and J. Horner, "Clutter effects on optical correlators," in *Optical Information Processing Systems and Architectures*, *Proc. Soc. Photo-Opt. Instrum. Eng.* **1151**, 130–137 (1989).
24. S. Almedia and G. Indebetouw, "Pattern recognition via complex spatial filtering," in *Applications of Optical Fourier Transforms*, H. Stark, ed. (Academic, New York, 1982), p. 60.
25. J. Khoury, P. D. Gianino, J. S. Kane and C. L. Woods, "Edge-enhancement techniques for improving the performance of binary phase-only filter pattern-recognition devices," *Opt. Eng.* **33**, 856–864 (1994).
26. We tested<sup>1,2,3</sup> sampling each pixel from 1 point  $\times$  1 point to 4 points  $\times$  4 points and found that 2 points  $\times$  2 points were adequate to sample SLM's with no dead zone.